# Ultrafast Vibrational Dynamics in a Quasi-One-Dimensional System: Femtosecond Impulsive Excitation of the PtBr(ethylenediamine) Mixed-Valence Linear Chain Complex

**S. L. Dexheimer* and A. D. Van Pelt**

*Department of Physics, Washington State University, Pullman, Washington 99164-2814*

**J. A. Brozik[†] and B. I. Swanson**

*Chemical Science and Technology Division, Los Alamos National Laboratory, Los Alamos, New Mexico 87545*

*Received: October 29, 1999; In Final Form: February 24, 2000*

We have used femtosecond impulsive excitation to time-resolve the vibrational motions following the excitation of the optical intervalence charge transfer transition in a quasi-one-dimensional molecular solid, the mixed-valence metal−halide linear chain complex $[Pt(en)_2][Pt(en)_2Br_2]\cdot(PF_6)_4$ (en = ethylenediamine, $C_2H_8N_2$). Wavelength-resolved measurements reveal an induced absorption signal assigned to the formation of the self-trapped exciton that is strongly modulated by vibrational wavepacket oscillations originating on both the ground and excited electronic states. The ground-state response, which includes the fundamental chain axis symmetric stretch frequency and its harmonics, is discussed in terms of resonantly enhanced impulsive stimulated Raman excitation of a strongly coupled electron−phonon system.

## I. Introduction

Femtosecond impulsive excitation techniques have revealed a wealth of information about ultrafast vibrational dynamics in molecular and condensed matter systems. In this paper, we report studies of the vibrational dynamics associated with photoexcitation of a quasi-one-dimensional molecular solid, the halogen-bridged mixed-valence transitional metal linear chain complex $[Pt(en)_2][Pt(en)_2Br_2]\cdot(PF_6)_4$, (en = ethylenediamine, $C_2H_8N_2$), also abbreviated as PtBr(en). In our previous paper on this system,[1] we analyzed the excited-state vibrational dynamics in terms of the lattice motions associated with the formation of the self-trapped exciton, a photoinduced structural change inherent to quasi-one-dimensional systems. In this paper, we discuss in more detail the ground-state vibrational dynamics of this strongly coupled electron−phonon system, which are manifested as large-amplitude wavepacket oscillations with strong overtone components.

Halogen-bridged mixed-valence transitional metal chain (MX) complexes have attracted considerable interest as model systems for studying the physics of quasi-one-dimensional solids.[2,3] The essential elements of the one-dimensional structure are indicated in Figure 1a, which shows both the periodic charge disproportionation (or mixed-valence character) and the periodic bond length distortion (or Peierls distortion) characteristic of the charge density wave ground state. An important aspect of the utility of the MX materials as model systems lies in their chemical tunability: for example, the bridging halide has a profound effect on the strength of the electron−phonon coupling, and with it, the strength of the charge density wave state. As the halide in the platinum complexes is varied through the series Cl, Br, and I, the strength of the electron−phonon interaction varies from very strong coupling in the highly distorted, valence-localized PtCl system to much weaker coupling in the valence-delocalized PtI system. The structure and dynamics of the electronically excited states of these systems are also dominated by the strength of the electron−phonon couplings. In the MX complexes, as in many other quasi-one-dimensional systems, strong electron−phonon interactions can lead to the formation of nonlinear excitations such as self-trapped excitons, in which electronic excitations are localized as a result of lattice distortions that occur in response to the excitation. The schematic structure of the self-trapped exciton (STE) state is shown in Figure 1b. In this figure, the STE is represented by two adjacent $M^{3+}$ ions; the actual spatial extent of the localized excitation is largely determined by the strength of the electron−lattice interaction in a particular material.

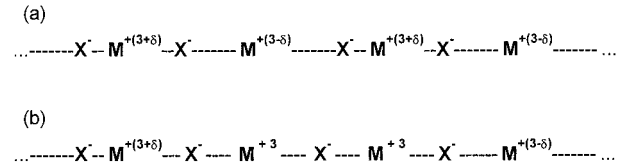


**Figure 1.** (a) Schematic ground-state structure of the halogen-bridged mixed-valence transitional metal linear chain complexes, neglecting the transverse ligands and counterions. The metal ion M = Pt, Pd, or Ni and the halide ion X = Cl, Br, or I. (b) Schematic structure of the self-trapped exciton state resulting from structural relaxation following excitation of the optical intervalence charge transfer transition.

The vibrational spectra of the MX complexes reflect their quasi-one-dimensional nature. The MX complexes have been extensively studied using Raman and infrared spectroscopies.[4] The optically active chain-axis vibrational modes, which dominate the vibrational response, are shown in Figure 2. The three optically active modes include one Raman-active mode ($\nu_1$), which is a fully symmetric stretching mode in which the halide ions are symmetrically displaced about the metal ions, and two infrared-active modes, consisting of an asymmetric stretching mode ($\nu_2$) that involves displacements of the halide ions about the metal ions, and a low-frequency mode ($\nu_3$) that involves relative motion of the inequivalent metal ions. As

[†] Present address: Department of Chemistry, University of New Mexico, Albuquerque, NM 87131.

10.1021/jp993859f CCC: $19.00 
Published on Web 04/19/2000

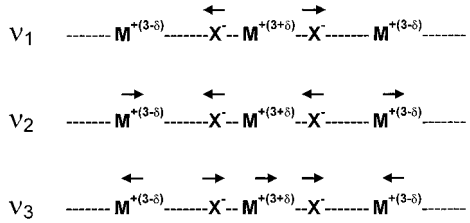


**Figure 2.** Optically active chain-axis vibrational modes for the metal-halide chain complex.

expected, a number of weaker modes associated with the transverse structure are also present.

The optical absorption spectrum is typically dominated by a strong intervalence charge transfer (IVCT) transition. This transition, which is highly polarized along the chain axis, transfers charge density between inequivalent metal ions, effectively acting to locally reverse the charge density wave. Since the equilibrium metal−halide bond lengths depend on the charge distribution about the metal ions, the IVCT transition is strongly coupled to the Raman-active symmetric stretching mode ($\nu_1$), resulting in substantial vibronic broadening of the absorption band. Excitation of the IVCT band creates a highly nonequilibrium lattice configuration that subsequently relaxes to form localized nonlinear excitations, and generation of self-trapped excitons, solitons, and polarons has been predicted theoretically.[2,5−7] In an ideal one-dimensional system, the excited-state self-trapping process is expected to be barrierless, resulting in rapid dynamics.[8] The initial relaxation processes leading to the formation of the STE are thought to occur on a femtosecond time scale, consistent with the idea that chain-axis vibrational motions directly drive this process.

Given the properties discussed above, quasi-one-dimensional materials are promising systems for investigating the interplay of the electronic and vibrational processes in ultrafast dynamics. The quasi-one-dimensional structure of these materials simplifies the dynamics in that the dominant motion is expected to occur along the linear axis, and the chemical tunability of the MX complexes allows direct control over the relevant electron−phonon interactions. Moreover, the relevant chain axis motions in these materials are relatively slow (∼100 fs or more in period), allowing the vibrational dynamics to be resolved in detail. It is interesting to note that the mixed-valence linear chain complexes can be thought of as extended analogues of the binuclear mixed-valence transition metal complexes that have provided a great deal of insight into the mechanism of electron transfer processes.[9] Thus, comparison of the dynamics of the extended-state and binuclear systems may contribute to a more general understanding of charge transfer processes.

To directly probe the vibrational processes coupled to the IVCT transition, we have used femtosecond impulsive excitation techniques. When a material is excited with optical pulses short compared to the periods of its characteristic vibrations, the vibrational modes coupled to the excited electronic transition are impulsively excited, creating vibrational wavepackets that consist of coherent superpositions of vibrational states.[10−13] These nonstationary vibrational wavepackets, which can be formed on both the ground and excited potential energy surfaces, oscillate at the characteristic vibrational frequencies of the material and are observable as a time-dependent modulation of the optical response. Impulsive excitation methods are especially useful for studying vibrational dynamics associated with electronic excitation, since only the vibrations that are coupled to the electronic transition are excited. The evolution of the resulting wavepacket oscillations directly reflects the nuclear dynamics, providing a means to observe the role of specific vibrational modes in fast photoinduced processes. An important aspect of vibrationally impulsive excitation experiments is the possibility of detecting both excited- and ground-state vibrational motions, in contrast to cw Raman spectroscopy, which detects only ground-state vibrational frequencies. Since it is crucial to be able to distinguish between ground- and excited-state motions to definitively interpret the measurements, a thorough understanding of both the ground- and excited-state vibrational response is required.

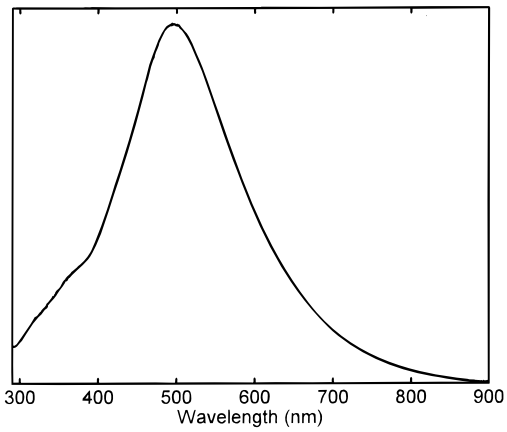


**Figure 3.** Optical response of $[Pt(en)_2][Pt(en)_2Br_2]\cdot(PF_6)_4$, as measured by diffuse reflectance, showing the strong intervalence charge transfer transition.

In this paper, we present time-resolved studies of the vibrational dynamics of PtBr(en), an MX complex with an electron−phonon coupling of intermediate strength. The chain-axis lattice distortion in PtBr(en) can be characterized by a ratio $\rho \sim 0.8$ between the short and long metal halide bonds.[3] In addition to the bromide bridging ligands along the chain axis, each platinum ion is coordinated by two transverse ethylenediamine units, which provide a nearly square-planar geometry. In the crystalline form, the material is strongly dichroic, with chains oriented parallel to the crystal axis. The chains are separated by $PF_6$ counterions, which provide overall charge neutrality and act to spatially separate the chains so that they experience minimal interchain interactions.

The optical response of PtBr(en), as measured by diffuse reflectance, is shown in Figure 3. The dominant feature is the IVCT transition, which is centered at ∼500 nm, and which is markedly broadened as a result of the strong vibronic coupling to the Raman-active chain-axis vibrational mode. At room temperature, the long-wavelength side of the absorption spectrum has a long tail that extends beyond 800 nm. Resonance Raman measurements show a strong peak at ∼180 $cm^{-1}$, corresponding to the symmetric stretch mode, as well as progressively weaker overtones at the second and third harmonic frequencies of this motion.[14]

## II. Experimental Section

Measurements of the time-resolved differential transmittance[15] were made using standard femtosecond pump−probe techniques. The optical pulses used in the measurements were derived from a laser system consisting of a home-built ∼10 fs Ti:S oscillator[16] that seeds a Coherent/BMI α-1000/US regenerative Ti:S amplifier operating at a repetition rate of 1 kHz. Output pulses from the amplifier are 35 fs in duration with a center wavelength of 800 nm and a spectral width (fwhm) of ∼30 nm. Measurements were carried out in one of two configurations: the degenerate pump−probe configuration, in which identical pulses are used

for both the pump and the probe, and the continuum probe configuration, in which the probe is derived from a broadband femtosecond continuum. In both cases, the 35 fs, 800 nm pulses generated by the amplifier were used as pump pulses. The femtosecond continuum was generated by splitting off a portion of the amplifier output and focusing it into a 2 mm thick sapphire plate. The near-infrared part of the continuum was compressed using a dispersive delay line constructed of fused silica prisms, giving a cross-correlation width of ~50 fs over the detected wavelength ranges. In both pump−probe configurations, wavelength resolution was achieved by spectrally filtering the probe pulse using a ~10 nm bandwidth interference filter after the pulse was transmitted through the sample.

The experimental samples were single crystals of $[Pt(en)_2][Pt(en)_2Br_2]\cdot(PF_6)_4$ of good optical quality. Recent advances in the synthesis of the metal−halide complexes have resulted in the production of materials that are largely free of defects and that are resistant to photoinduced damage.[17] Since the optical transitions are strongly polarized, the samples were oriented so that the molecular chain axis was parallel to the polarization of both the pump and probe pulses. Care was taken to ensure that a pump−probe response was absent at negative delay times (i.e., when the probe pulse precedes the pump), since such a signal could be indicative of the generation of long-lived photoinduced defects in the material.

The impulsive excitation signals are expected to have a temporal dependence given by a sum of exponentials and exponentially damped cosinusoids:

$$S(t) = \sum_i a_i e^{-t/\tau_i} \cos(2\pi\nu_i t + \phi_i)$$

where simple exponential decays are included as zero-frequency components. The differential transmittance signals were fit to this functional form using both linear prediction/singular value decomposition (LPSVD)[18] and traditional nonlinear least-squares methods. The two methods generally gave consistent results, though the LPSVD results tended to more accurately extract the damped oscillatory components, whereas the nonlinear least-squares fits tended to provide more consistent values for nonoscillatory exponential components.

## III. Results

Time-resolved differential transmittance measurements following excitation of the PtBr(en) complex near the onset of the IVCT optical absorption band are shown in Figure 4. The 35 fs duration pump pulses are sufficiently short to impulsively excite the ~180 $cm^{-1}$ (185 fs period) symmetric stretch chain axis mode of the complex. The measurements shown in Figure 4 were taken in the degenerate pump−probe configuration, and the spectral component of the probe pulse around 830 nm, on the red side of the pulse spectrum, was detected. As can be seen in the figure, the time-resolved response is modulated by wavepacket oscillations of unusually large amplitude. Beneath the oscillations, an induced absorbance signal appears on a time scale of ~100 fs, corresponding to the self-trapped exciton that is created in the excited electronic state.

The frequency content of the oscillatory response can be determined by Fourier analysis, and Figure 5 shows the Fourier power spectrum of the oscillatory part of the data trace shown in Figure 4. The exponentially varying baseline was subtracted prior to Fourier transformation. A strong peak at ~175 $cm^{-1}$ is the dominant feature in the Fourier power spectrum. This frequency coincides, within the combined experimental errors,

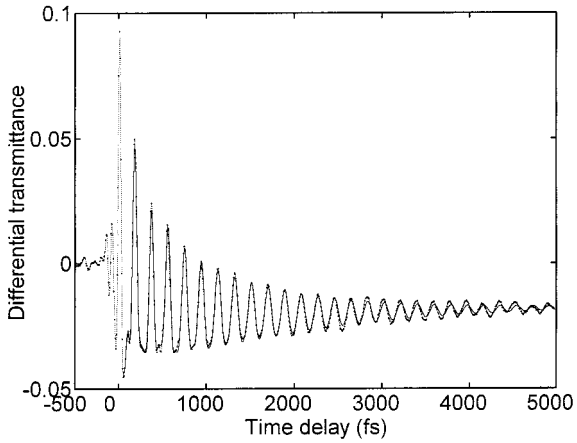


**Figure 4.** Measurement of the time-resolved differential transmittance of $[Pt(en)_2][Pt(en)_2Br_2]\cdot(PF_6)_4$ following impulsive excitation near the onset of the IVCT band using pulses 35 fs in duration centered at 800 nm. The measurement was taken in the degenerate pump−probe configuration with a detection wavelength of 830 nm. Data points are displayed as solid circles connected by dashed lines. The solid line represents a fit to the data using the LPSVD method discussed in the text, with parameters shown in Table 1.

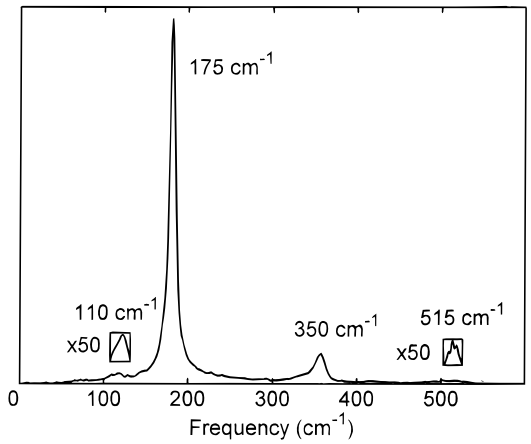


**Figure 5.** Fourier power spectrum of the oscillatory part of the time-resolved differential transmittance shown in Figure 4, showing frequency components at 110, 175, 350, and ~515 $cm^{-1}$.

with the ~180 $cm^{-1}$ frequency in the resonance Raman spectrum that is assigned to the symmetric stretch chain axis mode. Additional Fourier peaks are evident at frequencies of ~350 and ~515 $cm^{-1}$, which are also observed in the Raman spectrum and correspond to the second and third harmonics of the symmetric stretch mode. An additional feature at a frequency of ~110 $cm^{-1}$ in the Fourier power spectrum is not observed in the Raman spectrum. As discussed in our previous work,[1] this feature is much more prominent at detection wavelengths lying farther into the STE absorption band, and the spectral and temporal dependence of this frequency component is consistent with an excited-state wavepacket response.

The components of the data were determined quantitatively using LPSVD fits, and the resulting fit parameters are presented in Table 1. The data were fit starting at a delay time of ~65 fs to avoid contributions from coherent effects that may occur during the temporal overlap of the pump and probe pulses. Four oscillatory components are evident at frequencies that correspond, within experimental uncertainty, to the frequencies identified in the Fourier power spectrum. In addition, two zero-frequency components, which correspond to simple exponentials, appear in the fit results. The faster component follows the formation of the induced absorbance signal assigned to the

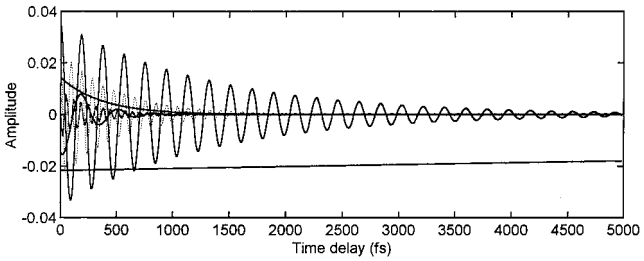


**Figure 6.** Individual damped oscillatory and exponential components reconstructed from the LPSVD analysis of the data trace displayed in Figure 4. The components correspond to the parameters given in Table 1.

**TABLE 1: LPSVD Fit Parameters for the Differential Transmittance Data Presented in Figure 4**

| freq ($cm^{-1}$) | $\tau$ (fs) | $\phi$ (deg) | amplitude |
|---|---|---|---|
| 0 | 370 | | 0.014 |
| 0 | 26000 | | 0.022 |
| 103 | 240 | 149 | 0.0085 |
| 176 | 1300 | 9 | 0.018 |
| 351 | 510 | 17 | 0.012 |
| 510 | 210 | 80 | 0.0043 |

STE state. The slower rising component is not well determined in this 5 ps long data trace, and most likely includes contributions from the decay of the STE population (see below) as well as from vibrational relaxation. The structure of the components of the signal can be seen in Figure 6, which displays the individual components as reconstructed from the LPSVD fit parameters. The sum of these components, i.e., the full LPSVD fit, is shown superimposed on the data trace in Figure 4.

To more clearly investigate the dynamics, additional time-resolved measurements were taken using the continuum probe configuration at a series of detection wavelengths extending farther into the red-shifted STE absorption band. Time-resolved differential transmittance measurements at detection wavelengths of 830, 880, and 940 nm are presented in Figure 7a−c. The data at 830 nm is presented to show the effect of the slightly lower time resolution of the continuum probe measurements relative to the degenerate pump−probe measurements. Comparison of the response in Figure 7a to the degenerate pump−probe measurement in Figure 4 indicates that essentially the same features are present in both measurements, although the lower time resolution results in a lower oscillation amplitude for the fundamental symmetric stretch frequency and significantly damps the harmonic response.

The time-resolved differential transmittance at 880 nm clearly shows a large induced absorbance signal associated with the STE state. Neglecting coherence effects around zero delay time, the formation time fits to an exponential time constant of ∼250 fs, and the decay of the induced absorbance fits to a time constant of ∼7 ps. The signal at 880 nm is modulated by oscillations at the chain axis symmetric stretching mode at ∼175 $cm^{-1}$, although the amplitude of the oscillations is significantly lower than that detected at 830 nm. The signal also shows marked structure at short times, and fits to the data reveal that the structure results from beating between the 175 $cm^{-1}$ mode and a large-amplitude, strongly damped component at ∼110 $cm^{-1}$, the same frequency detected at lower amplitude in the response at 830 nm.

The detection wavelength of 940 nm lies essentially outside the IVCT absorption band, but lies well into the STE absorption, as seen in the observed induced absorbance signal. A weak modulation at the chain axis symmetric stretch mode frequency of ∼175 $cm^{-1}$ is still evident in the response. The structure in

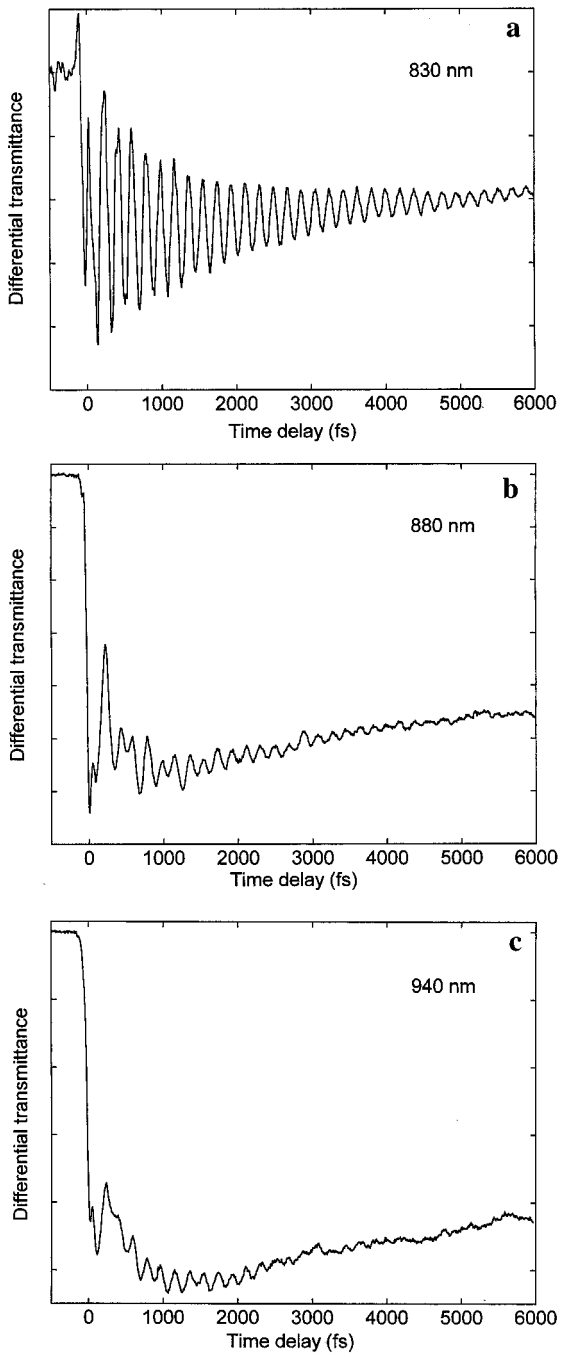


**Figure 7.** Time-resolved differential transmittance measurements of $[Pt(en)_2][Pt(en)_2Br_2]\cdot(PF_6)_4$ taken in the continuum probe configuration at detection wavelengths of (a) 830 nm, (b) 880 nm, and (c) 940 nm.

the signal at short times again results from beating between the 175 $cm^{-1}$ mode and the strongly damped component at ∼110 $cm^{-1}$. The difference in the details of the structure at 880 nm and at 940 nm results largely from the phase evolution of the low-frequency component as a function of detection wavelength.

## IV. Discussion

In order to interpret the wavepacket response in terms of the detailed vibrational dynamics, the origin of the individual oscillatory components in the time-resolved response must be identified. Since the electronic dephasing in this condensed phase system is expected to be extremely fast, we can effectively characterize the observed oscillatory modulations following the pump pulse in terms of distinct contributions from the ground

and excited electronic states. In the molecular complex studied in this work, it is possible to distinguish between ground-state and excited-state vibrational processes by comparison of the observed frequencies with those in the resonance Raman spectrum, and by careful investigation of the spectral dependence of the oscillatory response. In our previous work,[1] we presented a detailed analysis of the amplitude, damping time, and phase of the $\sim$110 $cm^{-1}$ component, which is not observed in the Raman spectrum, as a function of detection wavelengths extending well into the STE absorption band. As a result of this analysis, we identified this strongly damped low-frequency component as corresponding to the lattice motion that carries the system to the self-trapped configuration in the excited electronic state, providing a clear, unambiguous, observation of the dynamics of this important process.

The dominant contribution to the oscillatory response, which occurs at as frequency of $\sim$175 $cm^{-1}$, is consistent with a vibrational wavepacket in the ground electronic state: its frequency is close to that of the 180 $cm^{-1}$ chain-axis symmetric stretching mode identified by resonance Raman spectroscopy, and the observed damping time is consistent with the measured Raman line width. Excitation of the symmetric stretch mode by a resonantly enhanced impulsive stimulated Raman mechanism may be expected, given its strong coupling to the IVCT transition. As noted above, the wavepacket oscillations at $\sim$350 and $\sim$515 $cm^{-1}$ correspond to the second and third harmonics of the fundamental chain-axis symmetric stretching mode, allowing these components to be identified as higher-order vibrational coherences in the ground electronic state.

Two aspects of the ground-state vibrational response in PtBr(en) are particularly striking: the structure of the oscillatory response, in terms of its magnitude and harmonic content, and the observation of significant oscillatory modulation at detection wavelengths far to the red of the excited optical transition. Both of these effects may be understood in terms of the strong electron−phonon coupling in this system. The fundamental and two harmonic frequencies of the chain-axis symmetric stretching mode appear in both the resonance Raman spectrum and the oscillatory response, consistent with excitation of the strongly coupled mode by an impulsive stimulated Raman scattering mechanism. The unusual structure of the degenerate pump−probe signal at 830 nm results from the fundamental and second harmonic being excited nearly in phase: alternate peaks of the second harmonic interfere constructively with the peaks of the fundamental and destructively with the troughs of the fundamental, as can be seen in Figure 6. This interference leads to an effective sharpening of the wavepacket response. In PtBr(en), the harmonic components of the wavepacket response damp significantly faster than the fundamental component, which damps with an exponential time constant of $\sim$1.5 ps, a time scale typical of vibrational relaxation times in condensed phase materials. This behavior may be consistent with some degree of anharmonicity in the ground-state potential surface.

The observation of an oscillatory modulation at the ground-state vibrational frequency at detection wavelengths well outside the Franck−Condon region can also be understood in terms of the impulsive stimulated Raman mechanism. We note that impulsive excitation of coherent vibrational motion can result in modulation of both the real and imaginary components of the optical response, and that both of these effects can, in principle, contribute to an observable oscillatory modulation of the temporal response in a wavelength-resolved differential transmittance measurement. Hence, the oscillatory response at the ground-state vibrational frequencies may include contributions both from the time-dependent modulation of the real index of refraction, which may be resonantly enhanced,[13] as well as from the modulation of the absorption spectrum resulting from population of higher-lying vibrational levels in the ground electronic state. As shown in Figure 8, the resonant impulsive Raman mechanism generates a ground-state vibrational wavepacket that includes higher-lying vibrational levels that are not populated in thermal equilibrium, giving rise to a red-shifted component to the impulsively excited optical response. This process has been modeled in detail;[19,20] however, in PtBr(en), the effect may be particularly striking because of the large displacement of the Raman-active symmetric stretch in the IVCT transition. In addition, in this experiment, we have pumped the red side of the IVCT band, which will preferentially involve thermally populated vibrational levels above the vibrational ground state. (Note that, at room temperature, where these measurements were taken, $kT$ is slightly larger than the ground-state vibrational spacing.) Impulsive excitation originating from these higher-lying vibrational levels will result in wavepacket modulation at even longer wavelengths. The contribution of this modulation to the overall signal amplitude is expected to be much lower, however, since the higher-lying thermally populated vibrational levels account for a smaller fraction of the total ground-state population, and this is consistent with the observation of the substantially weaker wavepacket oscillations at the strongly red-shifted detection wavelengths of 880 and 940 nm.

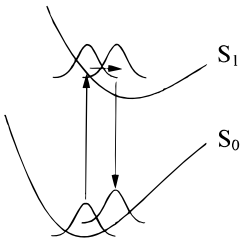


**Figure 8.** Schematic representation of the resonant impulsive stimulated Raman scattering mechanism for the generation of vibrational wavepackets in the ground electronic state.

In summary, we have investigated the impulsive excitation response of a strongly coupled, quasi-one-dimensional, electron−phonon system. The response can be understood in term of contributions from the excited electronic state, as well as strong modulation from vibrational coherence in the ground electronic state generated by a resonantly enhanced impulsive stimulated Raman mechanism. Additional experiments on MX complexes of varying electron−phonon coupling are in progress and are expected to complement this work.

**Acknowledgment.** This work was supported in part by the donors of the Petroleum Research Fund, administered by the American Chemical Society, by the National Science Foundation, through CAREER Award DMR-9875765, and by Washington State University. Work at Los Alamos was supported by the Division of Materials Science of the Office of Basic Science, US Department of Energy, and by the Los Alamos LDRD Program. We thank Keith Nelson for interesting discussions.

## References and Notes

(1) Dexheimer, S. L.; Van Pelt, A. D.; Brozik, J. A.; Swanson, B. I. *Phys. Rev. Lett.*, in press.

(2) Gammel, J. T.; Saxena, A.; Batistic, I.; Bishop, A. R.; Phillpot, S. R. *Phys. Rev.* **1992**, *B45*, 6408.

(3) Scott, B.; Love, S. P.; Kanner, G. S.; Johnson, S. R.; Wilkerson, M. P.; Berkey, M.; Swanson, B. I.; Saxena, A.; Huang, X. Z.; Bishop, A. R. *J. Mol. Struct.* **1995**, *356*, 207.

(4) Love, S. P.; Huckett, S. C.; Worl, L. A.; Frankcom, T. M.; Ekberg, S. A.; Swanson, B. I. *Phys. Rev.* **1993**, *B47*, 11 107, and references therein.
(5) Suzuki, M.; Nasu, K. *Phys. Rev.* **1992**, *B45*, 1605.
(6) Mishima, A.; Nasu, K. *Phys. Rev.* **1989**, *B39*, 5758.
(7) Mishima, A.; Nasu, K. *Phys. Rev.* **1989**, *B39*, 5763.
(8) Song, K. S.; Williams, R. T. *Self-Trapped Excitons*, 2nd ed.; Springer: New York, 1996; Vol. 105.
(9) Barbara, P. F.; Meyer, T. J.; Ratner, M. A. *J. Phys. Chem.* **1996**, *100*, 13148.
(10) Yan, Y.-X.; Gamble, E. B.; Nelson, K. A. *J. Chem. Phys.* **1985**, *83*, 5391.
(11) Pollard, W. T.; Lee, S.-Y.; Mathies, R. A. *J. Chem. Phys.* **1990**, *92*, 4012.
(12) Romero-Rochin, V.; Cina, J. A. *Phys. Rev.* **1994**, *A 50*, 763.
(13) Dhar, L.; Rogers, J. A.; Nelson, K. A. *Chem. Rev.* **1994**, *94*, 157.
(14) Brozik, J. A.; Shreve, A. P., unpublished results.
(15) Note that in the small signal limit, the differential transmittance is simply proportional to the differential absorbance.
(16) Asaki, M. T.; Huang, C. P.; Garvey, D.; Zhou, J.; Kapteyn, H. C.; Murnane, M. M. *Opt. Lett.* **1993**, *18*, 977.
(17) Brozik, J. A.; Bardeau, J. F.; Scott, B. L.; Swanson, B. I. *Inorg. Chem. Acta* **1999**, *294*, 275.
(18) Wise, F. W.; Rosker, M. J.; Millhauser, G. L.; Tang, C. L. *IEEE J. Quantum Electron.* **1987**, *QE-23*, 1116.
(19) Dexheimer, S. L.; Wang, Q.; Peteanu, L. A.; Pollard, W. T.; Mathies, R. A.; Shank, C. V. *Chem. Phys. Lett.* **1992**, *188*, 61.
(20) Pollard, W. T.; Dexheimer, S. L.; Wang, Q.; Peteanu, L. A.; Shank, C. V.; Mathies, R. A. *J. Phys. Chem.* **1992**, *96*, 6147.